Proc. Natl. Acad. Sci. USA
Vol. 93, pp. 3099–3104, April 1996
Biochemistry

Crystal structures of the trimeric human immunodeficiency virus type 1 matrix protein: Implications for membrane association and assembly

CHRISTOPHER P. HILL*, DAVID WORTHYLAKE, DANIEL P. BANCROFT, ALLYSON M. CHRISTENSEN, AND WESLEY I. SUNDQUIST*

Department of Biochemistry, University of Utah, Salt Lake City, UT 84132

Communicated by Stephen C. Harrison, Harvard University, Cambridge, MA, December 16, 1995 (received for review December 8, 1995)

ABSTRACT **The human immunodeficiency virus type 1 (HIV-1) matrix protein forms a structural shell associated with the inner viral membrane and performs other essential functions throughout the viral life cycle. The crystal structure of the HIV-1 matrix protein, determined at 2.3 Å resolution, reveals that individual matrix molecules are composed of five major helices capped by a three-stranded mixed β-sheet. Unexpectedly, the protein assembles into a trimer in three different crystal lattices, burying 1880 Å^2 of accessible surface area at the trimer interfaces. Trimerization appears to create a large, bipartite membrane binding surface in which exposed basic residues could cooperate with the N-terminal myristoyl groups to anchor the protein on the acidic inner membrane of the virus.**

The 55-kDa human immunodeficiency virus type 1 (HIV-1) Gag polyprotein contains all the information necessary to encapsidate the viral RNA genome, direct the assembly and budding of viral particles, and organize the envelope protein on the virion surface (for reviews see refs. 1–3). Genetic studies have established that the N-terminal matrix domain of Gag is responsible for membrane targeting (4–7) and envelope binding (8–11), whereas the downstream capsid and nucleocapsid domains contain the primary determinants for Gag assembly (12–17) and RNA encapsidation (18–23). As the assembling virion buds, Gag is processed by the viral protease to produce three discrete proteins: matrix (p17, residues 1–132), capsid (p24, 133–363), and nucleocapsid (p7, 378–432), as well as three smaller polypeptides. Proteolytic processing of Gag is necessary for subsequent maturation of the virion into an infectious viral particle. Viral maturation is characterized by a dramatic condensation of the capsid and nucleocapsid proteins into an electron dense cone surrounding the RNA genome, while the matrix protein remains behind in a shell associated with the inner face of the viral membrane (24–27).

The matrix polypeptide performs essential functions throughout the viral life cycle both as a domain of Gag (prior to proteolytic processing) and as a discrete protein (following processing). Mutational analyses have revealed that sequences near the N terminus of matrix are responsible for localizing the assembling Gag protein to the inner leaflet of the cell membrane. Both the N-terminal myristoyl group (4, 5) and a series of basic residues within the first 50 amino acids of matrix are required for the membrane localization of Gag (6, 7). Tight membrane binding therefore appears to require both insertion of the myristoyl group into the lipid bilayer and ionic interactions between the basic matrix residues and the acidic membrane surface (28, 29). The matrix domain of Gag also appears to organize the transmembrane subunit (TM; gp41) of the envelope protein on the surface of the virus since envelope-deficient viral particles can result from mutations in either matrix or the intracellular domain of TM (8–11).

The processed matrix protein participates in the trafficking of the viral replication particle early in the viral life cycle. Large deletions within the C-terminal 27 amino acids of matrix result in viruses that assemble, bud, and mature normally but cannot productively infect a new cell (30). The C terminus of matrix is therefore dispensable for viral assembly but required for viral entry. Upon entry, a phosphorylated subset (≈1%) of matrix molecules are bound to viral integrase proteins and thereby remain stably associated with the viral genome during reverse transcription and nuclear localization (31, 32). In this context, matrix displays one of the two redundant nuclear localization signals responsible for uptake of the large proviral preintegration complex (33, 34). Proviral nuclear localization is unique to the lentiviral class of retroviruses and may allow HIV-1 to replicate in nondividing cells, including terminally differentiated macrophages (31, 33, 34) [although this conclusion has been disputed (35, 36)]. In an effort to understand the structural bases for the diverse functions of the matrix protein in the HIV-1 viral life cycle, we have determined the protein's structure in two different crystalline lattices.†

EXPERIMENTAL PROCEDURES

Matrix Protein Purification. Recombinant HIV-1 matrix protein (residues 0–132) was expressed and purified as described (37). Recombinant matrix was identical to authentic HIV-1_{NL4-3} matrix except for an additional N-terminal residue (His-0), the retention of Met-1, and the absence of an N-terminal myristoyl modification. Selenomethionyl (SeMet) matrix was produced by introducing a Leu-61 to Met mutation and expressing the protein in the methionine auxotroph B834(DE3) (38) grown in M9 minimal medium supplemented with selenomethionine (60 mg/liter). Quantitative incorporation of SeMet was confirmed by electrospray mass spectrometry.

Crystallization. Three different matrix crystal forms were grown under similar conditions at 4°C in sitting drops from a protein solution of matrix (11 mg/ml) in 10 mM Tris·HCl, pH 8.0/1 mM EGTA/5 mM 2-mercaptoethanol (Table 1). The drops contained equal volumes of protein and reservoir solutions. The reservoir solutions were as follows: form I, 30% (wt/wt) $PEG_{MME}2K$, 0.1 M $(NH_4)_2SO_4$, 0.1 M $Na(CH_3CO_2)$ (pH 5.0); form II, 30% (wt/wt) PEG 1.45K, 0.2 M $(NH_4)_2SO_4$, 0.2 M $Na(CH_3CO_2)$ (pH 4.9); form III, 30% (wt/wt) $PEG_{MME}2K$, 0.2 M $(NH_4)_2SO_4$, 0.05 M $Na(CH_3CO_2)$ (pH 4.0).

The publication costs of this article were defrayed in part by page charge payment. This article must therefore be hereby marked "*advertisement*" in accordance with 18 U.S.C. §1734 solely to indicate this fact.

Abbreviations: HIV-1, human immunodeficiency virus type 1; ncs, noncrystallographic symmetry; MIR, multiple isomorphous replacement.

*To whom reprint requests should be addressed.

†The atomic coordinates and structure factors have been deposited in the Protein Data Bank, Chemistry Department, Brookhaven National Laboratory, Upton, NY 11973 [reference 1HIW (structure coordinates) and R1HIVSF (structure factors)].

Table 1. Matrix crystal forms

Crystal form	Space group	Unit cell dimensions	Mols/ AU	dmin, Å
I	$P2_1$	a = 63.4 Å, b = 91.2 Å, c = 74.0 Å, β = 102.9°	6	2.3
II	$P6_122$	$a = b$ = 72.8 Å, c = 298.6 Å	3	2.85
III	P321	$a = b$ = 76.2 Å, c = 50.4 Å	1	5.0

Mol/AU, number of matrix molecules per asymmetric unit; dmin, maximum resolution of data.

Form I SeMet crystals grew after streak seeding with native crystals. The mercury derivative was prepared by soaking crystals in 7 mM thimerosal for 40 h. The selenate derivative was prepared by soaking crystals for 16 h in a reservoir solution containing $(NH_4)_2SeO_4$ in place of $(NH_4)_2SO_4$. Data were collected at −160°C following stepwise transfer to a cryoprotectant reservoir solution containing 32% $PEG_{MME}2K$ and 20% glycerol. Data were processed with the programs DENZO and SCALEPACK (39). Crystallographic computations were performed using programs from the CCP4 suite (40) except where noted.

Form I Crystal Structure Determination. Mercury and selenium (SeMet) sites were identified in Patterson and difference Fourier maps and refined with MLPHARE to a figure of merit of 0.52 at 5.0 Å. These sites revealed the noncrystallographic symmetry (ncs) of two trimers in the asymmetric unit. Averaging of the 5 Å multiple isomorphous replacement (MIR) map using ncs operators obtained from the heavy atom positions showed cylinders of density corresponding to α-helices. The matrix NMR structure (37) was used as a rough guide for constructing the initial molecular envelope but not directly for phase calculations. Subsequent density modification (subunit averaging, solvent flattening, and histogram shifting) with the program DM resulted in a map that was readily interpretable even at 3.5 Å resolution. Iterative improvements were made to the molecular envelope and ncs operators as the model building and refinement progressed. Model phased difference Fourier maps were used to add and reject some minor heavy atom sites and to locate selenate anions. Subsequent heavy atom refinement and density modification (Tables 2 and 3) gave an experimental map of high quality (see Fig. 1*A*).

Table 2. Data statistics

	N(I)	Hg	SeMet	Se	N(II)
dmin, Å	2.3	3.0	4.07	3.0	2.85
Obs. refs.	104,117	55,523	23,770	37,137	65,134
No. refs.	36,171	15,797	6,579	15,569	11,282
Complete, %	98.4	92.3	89.1	91.6	97.2
R_{sym}, %*	8.2	5.8	4.1	6.2	4.9
$\langle I/\sigma(I)\rangle$	7.7	22.6	20.6	17.2	21.0
R_{iso}†		19.3	20.5	11.5	
R_c‡		0.68	0.79	0.89	
PPc§		0.83	0.67	0.43	
PPa		1.33	0.97	0.63	

N, native; Hg, thimerosal derivative; SeMet, selenomethionyl derivative; Se, Selenate soaked derivative. Statistics are for form I crystals except for N(II), which is the native data for form II crystals. Native data for form I crystals were collected to 2.5 Å on an RAXIS/RU200 and to 2.3 Å on a MAR detector at SSRL7.1. These two data sets were combined in SCALEPACK to give the data set used in phasing and refinement calculations. All other data were collected on an RAXIS/RU200 except for the form II data, which were collected on a MAR detector at SSRL7.1. dmin, maximum resolution of data; Obs. refs., no. of observed reflections; No. refs., number of unique references.

*$R_{sym} = 100\Sigma_{hkl}\Sigma_i|I_i\text{-}\langle I\rangle| / \Sigma\langle I\rangle$, where I_i is the intensity of a particular symmetry-related reflection.

†$R_{iso} = 100\Sigma(||F_{PH}| - |F_P||/\Sigma|F_P|)$, where F_P and F_{PH} are structure factor amplitudes of native and derivative.

‡$R_{Cullis} = \Sigma||F_{PH}{}^+/-F_P| - F_{H(calc)}|/\Sigma|F_{PH} - F_P|$, where the summation is over centric reflections.

§Phasing power (PPc centric, PPa acentric) = $(\Sigma(|F_H|^2/\Sigma|E|^2)^{1/2}$, where F_H is the structure factor of the heavy atoms and E (lack of closure error) = $|F_{PH(obs)}| - |F_{PH(calc)}|$.

Table 3. Refinement statistics

	Crystal form I	Crystal form II
Resolution, Å	8–2.3	8–2.85
⟨FOM⟩* (before DM)	0.42 (10–3.0Å)	
⟨FOM⟩ (after DM)	0.80 (10–2.5Å)	
R_{factor} (%)†	25.9	28.0
R_{free} (%)‡	33.2	38.5
Res (total)/H_2O/SO_4	658 (798)/70/8	313 (399)/0/0
rmsd bond lengths, Å	0.012	0.009
rmsd bond angles, °	1.67	1.24
⟨*B*⟩ (solvent), Å^2	27.7 (19.9)	24.2

*Mean figure of merit = $\langle|\Sigma P(\alpha)i^{i\alpha}/\Sigma P(\alpha)|\rangle$.

†$R_{factor} = 100\Sigma(||F_{P(obs)}| - |F_{P(calc)}||/\Sigma|F_{P(obs)}|$.

‡$R_{free} = R_{factor}$ for a randomly selected subset (5%) of the data that have not been used for minimization of the crystallographic residual.

Refinement. Atomic refinement was performed with X-PLOR (41) using simulated annealing, positional and B-factor refinement interspersed with rounds of rebuilding using the program O (42). Ordered residues for the six independent molecules are as follows: A, 7–121; B, 7–116; C, 7–119; A′, 7–118; B′, 7–109; C′, 7–111. An unassigned 53 Å-long tube of density was observed in the MIR/DM map and at >2.5σ in the final $F_o - F_c$ map. We speculate that this featureless density, which wraps about Trp-36 and Trp-36′ and extends into hydrophobic grooves atop the A and A′ molecules, may be an ordered PEG molecule binding in the site normally occupied by myristate when matrix is not membrane associated. An analogous situation has been observed for cAMP-dependent kinase, where a detergent molecule in the unmyristoylated protein structure partially fills the normal myristate binding site (43).

While the *R* factor (25.9% on all 2.3 to 8.0 Å data) is higher than usual for protein structures at 2.3 Å resolution, this probably results largely from the unassigned PEG density and the conservative number (70) of assigned water molecules in the model. Inclusion of only the most reliable water molecules is reflected in the relatively low *B* value for solvent (see Table 3). In addition, 140 residues (18% of total) have been omitted from the model because they lack defined density. These residues may have partial order and thus may contribute to the high *R* factor. A number of criteria establish the correctness of the structure: (*i*) The experimental electron density map is of high quality. (*ii*) All 598 non-Gly residues in the asymmetric unit have φ and ψ angles within the allowed region of a Ramachandran plot, except residues 45 of B and 110 of C′, which are both within the generously allowed region. (*iii*) The refined model shows good agreement with expected residue environments as judged by an average 3^D-1^D profile score of 0.52 and a minimum of 0.30 for an 11-residue window (44). (*iv*) The heavy atom positions are consistent with the expected structure; i.e., the six selenium positions in the SeMet crystals are found at the δ side chain positions of all six Met-61 residues and the eight mercuries are found covalently coordinated to cysteine sulfur atoms. (*v*) The real space correlation coefficients of the refined model with the MIR density modified map are 83.4% (main chain atoms) and 70.7% (side chain atoms). (*vi*) The overall matrix crystal structure agrees well with the NMR structures.

Form II Crystal Structure Determination. Data collection from a form II crystal was as described for form I crystals. The structure was determined by molecular replacement with AMoRE using the form I trimer as the search model. Form II crystals contain one trimer in the asymmetric unit with the ncs threefold axis parallel to the crystallographic *c* axis. Preliminary refinement and inspection of simulated annealing omit

maps indicates that form I and form II trimers are identical at this resolution.

RESULTS AND DISCUSSION

Three different crystal forms of the HIV-1 matrix protein were obtained, two of which diffract to high resolution (Table 1). The $P2_1$ matrix crystal structure was solved at 2.3 Å resolution by MIR and was subsequently used to solve the $P6_122$ structure at 2.85 Å resolution by molecular replacement. The $P2_1$ crystal form contains six matrix molecules in each asymmetric unit (designated A,B,C and A′,B′,C′), arranged as two independent trimers. The six crystallographically independent matrix molecules are very similar and align with pairwise rmsd of 0.29–0.79 Å (C^α 7–109). The $P6_122$ crystal form also contains a single copy of the same matrix trimer. The third crystal form, space group P321, shows a clear relationship in unit cell parameters to the $P6_122$ crystals, strongly suggesting that the same noncrystallographic trimer of the $P2_1$ and $P6_122$ crystals also occurs as a crystallographic trimer in the P321 crystal form. We observe no significant differences between the structures of individual matrix molecules in the $P2_1$ and $P6_122$ crystal forms and therefore describe only the $P2_1$ structure in detail.

The first 104 amino acids of the matrix protein form a single globular domain composed of five major helices (1-5) and capped by a three-stranded mixed β-sheet (strands 1–3) (Fig. 1 *B* and *C*). The structure is organized about a central, buried helix (helix 4, red), which spans the domain and makes hydrophobic contacts with all the other secondary structural elements, including an extensive antiparallel interaction with helix 3. Exposed basic residues in the cationic globular domain are strikingly clustered about the mixed β-sheet (Lys-15, Lys-18, Arg-20, Arg-22, Lys-26, Lys-27, Lys-39, Lys-95, and Lys-98) and the exposed face of helix 2 (Lys-32, Lys-39, and Arg-43). This basic patch functions as both the protein's membrane binding surface (6, 7) and nuclear localization signal (33, 34). Helix 5 projects away from the packed helical bundle (Fig. 1*C*), making the C-terminal 28 residues structurally distinct from the rest of the protein. The structure therefore rationalizes why deleterious mutations and deletions throughout the first 104 amino acids of matrix have different phenotypes (aberrant assembly, membrane binding, envelope binding, or nuclear localization) from deleterious deletions near the C terminus (blocked viral entry).

The matrix crystal structures reported here generally agree well with previously reported NMR solution structures (37, 46). Average crystallographic C^α positions 7–109 align with our current lowest-penalty NMR structure with an rmsd of 1.9 Å. The C-terminal helix (5) is significantly longer in the crystal, however, and the loop connecting helices 3 and 4 positions (67–72) rearranges upon matrix trimerization (see below). The crystal structure also resolves differences between the two independently determined matrix NMR structures. In particular, helix 1, which was well defined in only one of the matrix NMR structures (37), is clearly observed in the crystal structure.

As noted previously (47), helices 2–5 of HIV-1 matrix superimpose upon helices 1–4 of interferon-γ (backbone atom rmsd = 2.9 Å) (48, 49). The proposed dimerization of matrix (47, 50) via an interlocking helical structure as seen for interferon-γ is prevented, however, by tight contacts between matrix helices 2–5 and the additional packing of helix 1 against helices 2 and 4. Instead, the HIV-1 matrix protein forms trimers in all three crystal forms (Fig. 2). The intersubunit trimer interfaces are hydrophilic and bury a total solvent accessible surface area of 1880 $Å^2$ (average, 627 $Å^2$ per interface). The interfaces are created by packing the L3 loop (including helix 2′) against the L4 loop, creating a series of intermolecular hydrogen bonds (Fig. 2*A*).

Although matrix trimerization was unexpected, the structure appears consistent with a number of morphological, genetic, and biochemical observations. A model orienting the matrix trimer on the viral membrane is shown in Fig. 3. In this orientation, the C-terminal fifth helices project downward from the flat triangular assembly, as if toward the center of the virus. This would leave the capsid and nucleocapsid polypep-

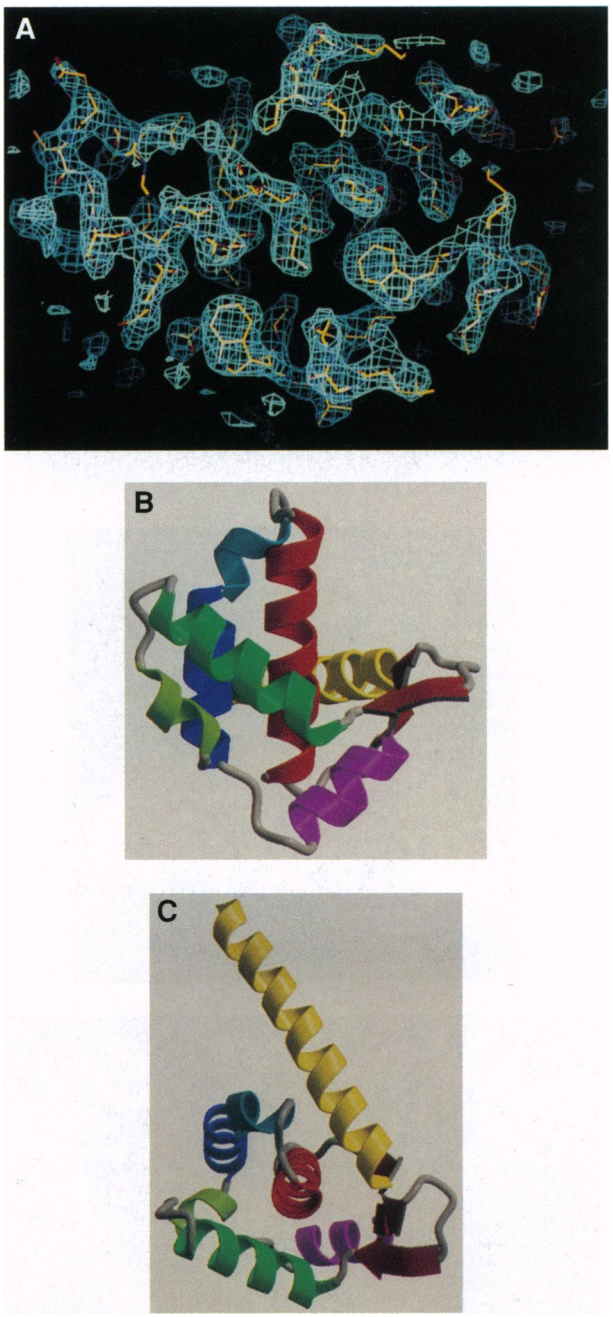

FIG. 1. (*A*) Density modified MIR map (blue), contoured at 1σ and shown superimposed upon the final refined model. (*B*) Ribbon diagram of the matrix monomer illustrating the globular domain and the structural role of the central fourth helix (red). Secondary structural elements of the representative A molecule are as follows (H, helix; S, strand; L, loop): H1, 11–19 (magenta); S1, 19–21 (orange); L1, 21–27 (gray); S2, 27–29 (orange); L2, 29–30 (gray); α-H2, 30–43 (green), L3, 43–47, 52–53 (gray); H2′, 47–52 (light green); H3, 53–64 (blue); H3′, 64–69 (light blue); L4, 69–72 (gray); H4, 72–89 (red); L5, 89–94 (gray); S3, 94–96 (orange); H5, 96–121 (yellow). H1–H5 are α-helical, H2′ is a 3_{10}-helix, and H3′ is a mixed $\alpha/3_{10}$-helix. The full amino acid sequence and numbering scheme for HIV-1_{NL4-3} matrix are given in ref. 37. Figs. 1 *B* and *C* and 2 were created using the programs MOLSCRIPT (45) and RASTER 3D (46). (*C*) Perpendicular view illustrating how the C-terminal fifth helix (yellow) projects away from the globular domain of the protein.

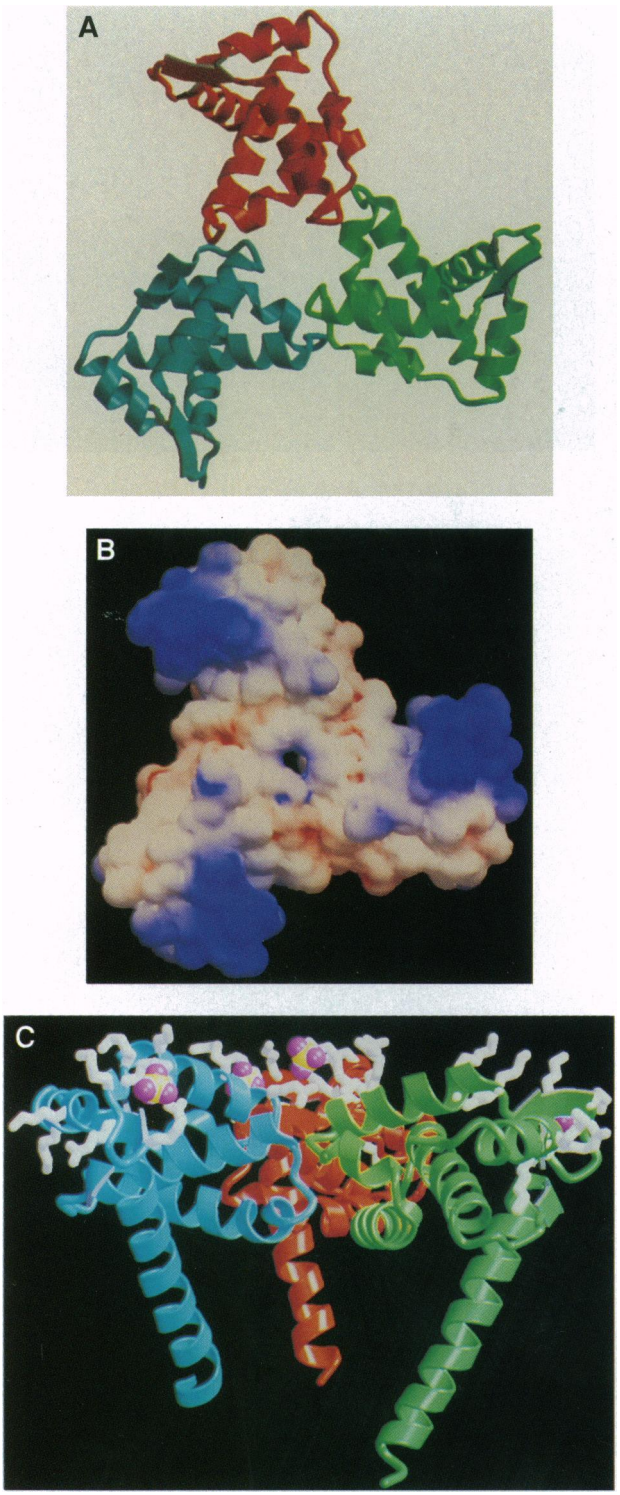

FIG. 2. Structures of the HIV-1 matrix protein trimer. (*A*) View of the triskelion-shaped matrix trimer down the threefold axis. Individual subunits are shown in red, blue, and green. The green subunit is rotated counterclockwise by approximately 30° in the plane of the paper with respect to the monomer of Fig. 1*B*. Trimer interfaces, which differ slightly in the conformations of surface sidechains, are created by packing residues 42–47, 59, and 63 against 69–74. Apparent hydrogen bonding interactions across the interfaces include: Ala-45O · · · Ser-72O$^{\gamma}$, Ala-45O · · · Ser-72N, Asn-47N · · · Thr-70O, Gln-63O$^{\varepsilon}$ · · · Thr-70O$^{\gamma}$, Gln-59O$^{\varepsilon}$/N$^{\varepsilon}$ · · · Gln-69O$^{\varepsilon}$/N$^{\varepsilon}$ (B · · · A, C · · · B, and A′ · · · C′ subunits only), Arg-43O · · · Arg-43N$^{\eta}$ (A · · · C and A′ · · · C′ only). In addition, the Ala-45C$^{\beta}$ methyl packs against the Phe-44 side chain across all of the trimer interfaces. (*B*) GRASP (51) drawing of the trimer shown in *A* illustrating the electrostatic surface potential on top of the matrix trimer. Surface was calculated using a 1.4-Å-radius probe and the potential is displayed in the range of −6 (red) to +6 (blue) *kT*. (*C*) View of the matrix trimer perpendicular to the threefold axis. Subunit color scheme is the same as in *A*. Basic side chains of the first 50 residues are shown in white. Four bound sulfate anions are shown in magenta and yellow. Three of the sulfates bind in basic pockets above the turn that links strands 1 and 2 (sites 1–3) and interact (S · · · N < 4.5 Å) with Arg-22N$^{\eta}$, Lys-26NH, and Lys-27NH. The fourth sulfate binds above the hole in the center of the trimer and interacts with Arg-43N$^{\eta 1}$ from A/A′ and C/C′ molecules, as well as Arg-39N$^{\eta 1}$ from a different trimer (site 4).

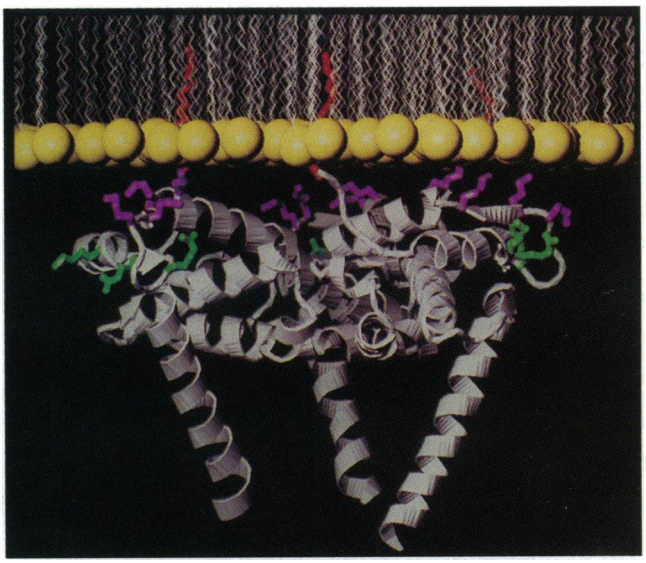

FIG. 3. Schematic model for matrix–membrane interaction. Side chains of basic residues that are essential (magenta) or nonessential (green) for optimal viral replication are shown (36). Arg-39 and Arg-43 (not shown) are also located on the top of the trimer and could interact with the membrane. The matrix myristates (to scale, red) are shown inserted into a stylized phospholipid membrane with the five N-terminal matrix residues and myristates placed in idealized positions.

tides free to condense toward the center of the virus following proteolytic processing at the C terminus of matrix. The model also suggests how the N-terminal myristoyl groups and N-proximal basic residues could act in synergy to stabilize the matrix trimer on an acidic membrane. In the proposed orientation, all three myristate aliphatic chains could insert into a lipid bilayer positioned above the trimer. Basic residues on the upper surface of the trimer would then be oriented to make ionic interactions with phospholipid head groups on the membrane surface (Fig. 3). In fact, this surface binds sulfate anions in the crystal. Four apparent sulfate binding sites were observed in initial maps of each trimer and confirmed in difference maps calculated from crystals soaked in ammonium selenate (Table 1). Three sulfates bind to individual matrix subunits over the open ends of the β-hairpins connecting strands 1 and 2, and a fourth sulfate binds just above the center of the trimer, making contacts with the A and C subunits (Fig. 2*C*).

Several studies have implicated the cluster of N-proximal basic residues in HIV-1 Gag membrane binding (6, 7). Recently, Freed and coworkers (36) have used site-directed mutagenesis to evaluate the importance of individual basic matrix residues in viral replication. Single and double amino acid substitutions of matrix residues Lys-18, Arg-20, and Arg-22 had no measurable effect on viral assembly and release in cultured HeLa cells, whereas substitutions at basic residues located immediately downstream (Lys-26, Lys-27, Lys-30, and Lys-32) reduced total virion production significantly. Locations of basic residues that are essential (magenta) or dispensable (green) for optimal viral replication are shown in Fig. 3. Strikingly, the essential basic residues are all located on the putative membrane binding surface of the trimer, whereas

nonessential basic residues are further removed from the membrane.

Although the matrix trimer appears to explain a number of important biological observations, the relevance of this structure for HIV-1 virion architecture and assembly remains to be elucidated. The role, if any, of matrix trimerization in viral assembly is not clear since the Gag protein preferentially assembles into higher-order oligomers (52–61) and since the major determinants for viral assembly map to the capsid and nucleocapsid domains of Gag (12–17). Nevertheless, a role for the matrix domain in Gag assembly is suggested by several observations: (*i*) mutations and deletions in central matrix residues (42–77), which span the trimerization contacts, can abolish viral assembly (8, 62, 63); (*ii*) expressed simian immunodeficiency virus matrix protein reportedly assembles and buds in the absence of any other viral proteins (64); and (*iii*) a peptide spanning matrix residues 47–59 (H2′, L3, and H3) inhibits the assembly of cultured virus (12). Although trimerization of the matrix domain could accompany higher-order Gag oligomerization, it is alternatively possible that matrix does not function as a trimer during viral assembly. In either case, we expect that as Gag assembles the orientation of the membrane binding "head" of matrix will be similar to that shown in Fig. 3.

The arrangement of matrix trimers in the $P6_122$ crystal lattice does bear a striking resemblance to one existing model for Gag assembly. Low-resolution electron microscopic studies of Gag molecules assembled on inner cell membranes led Nermut and coworkers (26, 27) to propose that Gag preferentially assembles into a two-dimensional lattice composed of interlocking six-membered rings, in which each ring shares single subunits with three neighboring rings. Their proposed lattice formally has p3 symmetry and a unit cell spacing of 66 ± 8 Å. We observe that matrix trimers in the *xy* plane of the $P6_122$ crystal form pack into an identical p3 lattice with a unit cell spacing of 72.8 Å. This lattice creates an array of large (≈1500 Å^2), threefold symmetric holes between matrix trimers. These holes are potential binding sites for the 17-kDa intracellular domain of the transmembrane envelope protein, which also appears to be a trimer (65–68) [although other oligomeric states have also been suggested (69–73)]. We do not, however, observe direct interactions between matrix trimers in the *xy* plane that would serve to stabilize this lattice on a two-dimensional membrane surface.

A more likely role for matrix trimerization is in constructing the matrix lattice of the mature HIV-1 virion. The outer lattice of the virus reportedly rearranges upon maturation (26), suggesting that matrix–matrix interactions may change as the subunits of Gag repack. Others have recently observed that trimers are the predominant multimeric state of matrix following glutaraldehyde-crosslinking in solution (L. Ehrlich and C. Carter, personal communication). Matrix–matrix interactions appear intrinsically weak, however, and our recombinant, unmyristoylated matrix protein is predominantly monomeric in solution, even at millimolar concentrations. Nevertheless, weak interactions could mediate matrix trimerization in the mature virion, where the nominal concentration of the ≈2000 copies of matrix in the 100-nm-diameter virion is ≈6 mM. Moreover, the effective local concentration of matrix will be much higher since the protein is concentrated and bound in a fixed orientation by the viral membrane. As shown in Fig. 3, the mutually compatible trimerization and membrane binding sites of matrix could therefore cooperate in assembling the mature viral matrix lattice.

In summary, the HIV-1 matrix protein consists of two structurally and functionally distinct regions: an N-terminal globular domain involved in protein assembly, membrane binding, and envelope incorporation, and a C-terminal region that projects away from the body of the protein and may play a role in viral entry. Matrix trimerization, which remains to be confirmed *in vivo*, appears to explain how the protein binds to the inner viral membrane and guides possible models for virion architecture. The crystal structure of the matrix trimer also provides the basis for designing new antiviral agents that inhibit assembly, disassembly, and/or membrane binding of the HIV-1 matrix protein shell.

Note Added in Proof. The x-ray crystal structure of the simian immunodeficiency virus (SIV) matrix protein was published after this manuscript was submitted and refereed (73). HIV-1 and SIV matrix share ≈50% sequence identity and the two proteins adopt very similar structures, except near their C-termini where the extended fifth helix of HIV-1 matrix is replaced by a β-hairpin structure in SIV matrix (residues 110–117). SIV MA also crystallized as a trimer that is essentially identical to the HIV-1 matrix trimer reported here, supporting our hypothesis that matrix trimerization is a fundamental feature of lentiviral assembly. Intriguingly, SIV matrix trimers crystallized in a planar p3 net that is similar to the trimeric arrays seen in HIV-1 MA crystal forms II and III.

Although the biological relevance of matrix trimerization remains to be established, several earlier reports favoring matrix dimerization have very recently been reinterpreted and are now consistent with trimerization. Balyaev *et al.* (74) initially reported that SIV matrix crystallized in space group C2, a result that was consistent with matrix dimerization but not trimerization. The C2 space group assignment has now been corrected, however, and the structure solved as a trimer in space group R3 (73). Similarly, Matthews *et al.* (47) initially proposed that HIV-1 matrix might form interlocked dimers based on an NMR model of the protein. However, their fully refined HIV-1 matrix structure contains an N-terminal helix (helix 1) that sterically precludes this dimerization mode (75). This helix is also seen in our crystal structure and in another HIV-1 MA NMR structure (37). A remaining discrepancy is a report that HIV-1 matrix protein forms dimers, rather than trimers, in solution (47).

We thank John Finch for helpful discussions; Matt Katus for technical assistance; Kevin Cowtan for advice on using the program DM; Lorna Ehrlich, Carol Carter, and Eric Freed for communicating their unpublished results; and Mike Summers, Venki Ramakrishnan, and members of our laboratories for critical reading of this manuscript. pNL4-3 DNA was obtained from M. Martin through the AIDS Research and Reference Reagent Program, Division of AIDS, National Institute of Allergy and Infectious Diseases, National Institutes of Health. This work was supported by National Institutes of Health Grant 1RO1AI37524 (to W.I.S. and C.P.H.), the Searle Scholars Program/Chicago Community Trust (W.I.S.), and a grant from the Lucille P. Markey Charitable Trust.

1. Wills, J. & Craven, R. (1991) *AIDS* **5,** 639–654.
2. Gelderblom, H. R., Bauer, P. G., Özel, M., Höglund, S., Niedrig, M., Renz, H., Morath, B., Lundquist, P., Nilsson, Å., Mattow, J., Grund, C. & Pauli, G. (1992) in *Membrane Interactions of HIV*, Aloia, R. C. & Curtain, C. C., eds. (Wiley–Liss, New York), pp. 33–54.
3. Linial, M. L. & Miller, A. D. (1990) *Curr. Topics Microbiol. Immunol.* **157,** 125–152.
4. Göttlinger, H. G., Sodroski, J. G. & Haseltine, W. A. (1989) *Proc. Natl. Acad. Sci. USA* **86,** 5781–5785.
5. Bryant, M. L. & Ratner, L. (1990) *Proc. Natl. Acad. Sci. USA* **87,** 523–527.
6. Yuan, X., Yu, X., Lee, T.-H. & Essex, M. (1993) *J. Virol.* **67,** 6387–6394.
7. Zhou, W., Parent, L. J., Wills, J. W. & Resh, M. D. (1994) *J. Virol.* **68,** 2556–2569.
8. Yu, X., Yuan, M., Lee, T.-H. & Essex, M. (1992) *J. Virol.* **66,** 4966–4971.
9. Dorfman, T., Mammano, F., Haseltine, W. A. & Göttlinger, H. G. (1994) *J. Virol.* **68,** 1689–1696.
10. Mammano, F., Kondo, E., Sodroski, J., Bukovsky, A. & Göttlinger, H. G. (1995) *J. Virol.* **69,** 3824–3830.
11. Freed, E. O. & Martin, M. A. (1995) *J. Virol.* **69,** 1984–1989.
12. Von Poblotzki, A. R., Wagner, M., Niedrig, G., Wanner, G., Wolf, H. & Modrow, S. (1993) *Virology* **193,** 981–985.
13. Chazal, N., Carriére, C., Gay, B. & Boulanger, P. (1994) *J. Virol.* **68,** 111–122.

14. Franke, E. K., Yuan, H. E. H., Bossolt, K. L., Goff, S. P. & Luban, J. (1994) *J. Virol.* **68,** 5300–5303.
15. Mammano, F., Öhagen, Å., Höglund, S. & Göttlinger, H. G. (1994) *J. Virol.* **68,** 4927–4936.
16. Dorfman, T., Bukovsky, A., Öhagen, Å., Högland, S. & Gottlinger, H. G. (1994) *J. Virol.* **68,** 8180–8187.
17. Reicin, A. S., Paik, S., Berkowitz, R. D., Luban, J., Lowy, I. & Goff, S. P. (1995) *J. Virol.* **69,** 642–650.
18. Aldovini, A. & Young, R. A. (1990) *J. Virol.* **64,** 1920–1926.
19. Gorelick, R. J., Nigida, S. M., Bess, J. W., Arthur, L. O., Henderson, L. E. & Rein, A. (1990) *J. Virol.* **64,** 3207–3211.
20. Luban, J. & Goff, S. P. (1991) *J. Virol.* **65,** 3203–3212.
21. Dorfman, T., Luban, J., Goff, S. P., Haseltine, W. A. & Göttlinger, H. G. (1993) *J. Virol.* **67,** 6159–6169.
22. Berkowitz, R. D., Luban, J. & Goff, S. P. (1993) *J. Virol.* **67,** 7190.
23. Jowett, J., Hockley, D., Nermut, M. V. & Jones, I. M. (1992) *J. Gen. Virol.* **73,** 3079–3086.
24. Gelderbloom, H. R., Hausmann, E. H., Özel, M., Pauli, G. & Koch, M. A. (1987) *Virology* **156,** 171–176.
25. Marx, P. A., Munn, R. J. & Joy, K. I. (1988) *Lab. Invest.* **58,** 112–118.
26. Nermut, M. V., Hockley, D. J., Jowett, J. B. M., Jones, I. M., Garreau, M. & Thomas, D. (1994) *Virology* **198,** 288–296.
27. Nermut, M. V., Grief, C., Hashmi, S. & Hockley, D. J. (1993) *AIDS Res. Hum. Retroviruses* **9,** 929–938.
28. Peitzsch, R. M. & McLaughlin, S. (1993) *Biochemistry* **32,** 10436–10443.
29. Resh, M. D. (1994) *Cell* **76,** 411–413.
30. Yu, X., Yu, Q.-C., Lee, T.-H. & Essex, M. (1992) *J. Virol.* **66,** 5667–5670.
31. Gallay, P., Swingler, S., Aiken, C. & Trono, D. (1995) *Cell* **80,** 379–388.
32. Gallay, P., Swingler, S., Song, J., Bushman, F. & Trono, D. (1995) *Cell* **83,** 569–576.
33. Bukrinsky, M. I., Haggerty, S., Dempsey, M. P., Sharova, N., Adzhubei, A., Spitz, L., Lewis, P., Goldfarb, D., Emerman, M. & Stevenson, M. (1993) *Nature (London)* **365,** 666–669.
34. von Schwedler, U., Kornbluth, R. S. & Trono, D. (1994) *Proc. Natl. Acad. Sci. USA* **91,** 6992–6996.
35. Schuitemaker, H., Kootstra, N. A., Fouchier, R. A. M., Hooibrink, B. & Miedena, F. (1994) *EMBO J.* **13,** 5929.
36. Freed, E. O., Englund, G. & Martin, M. A. (1995) *J. Virol.* **69,** 3949–3954.
37. Massiah, M., Starich, M. R., Paschall, C. M., Summers, M. F., Christensen, A. M. & Sundquist, W. I. (1994) *J. Mol. Biol.* **244,** 198–223.
38. Studier, F. W. & Moffatt, B. A. (1986) *J. Mol. Biol.* **189,** 113–130.
39. Otwinowski, Z. (1993) in *Data Collection and Processing*, eds. Sawyer, L., Isaacs, N. & Bailey, S. (Daresbury Laboratories, Warrington, U.K.), pp. 56–62.
40. Collaborative Computing Project 4 (1994) *Acta Crystallogr. D* **50,** 760–763.
41. Brunger, A. T. (1992) X-PLOR (Yale Univ., New Haven, CT), Version 3.1.
42. Jones, T. A., Zou, J., Y., Cowan, S. W. & Kjeldgaard, M. (1991) *Acta Crystallogr. A* **47,** 110–119.
43. Zheng, J., Knighton, D. R., Xuong, N.-H., Taylor, S. S., Sowadski, J. M. & Ten Eyck, L. F. (1993) *Protein Sci.* **2,** 1559–1573.
44. Luthy, R., Bowie, J. U. & Eisenberg, D. (1992) *Nature (London)* **356,** 83–85.
45. Kraulis, P. J. (1991) *J. Appl. Crystallogr.* **24,** 946–950.
46. Bacon, D. & Anderson, W. F. (1988) *J. Mol. Graphics* **6,** 219–220.
47. Matthews, S., Barlow, P., Boyd, J., Barton, G., Russell, R., Mills, H., Cunningham, M., Meyers, N., Burns, N., Clark, N., Kingsman, S., Kingsman, A. & Campbell, I. (1994) *Nature (London)* **370,** 666–668.
48. Samudzi, C. T., Burton, L. E. & Rubin, J. R. (1991) *J. Biol. Chem.* **266,** 21791–21797.
49. Ealick, S. E., Cook, W. J., Vijay-Kumar, S., Carson, M., Nagabhushan, T. L., Trotta, P. P. & Bugg, C. E. (1991) *Science* **252,** 698–702.
50. Morikawa, Y., Kishi, T., Zhang, W. H., Nermut, M. V., Hockley, D. J. & Jones, I. M. (1995) *J. Virol.* **69,** 4519–4523.
51. Nicholls, A., Sharp, K. A. & Honig, B. H. (1991) *Proteins* **11,** 281.
52. Karacostas, V., Nagashima, K., Gonda, M. A. & Moss, B. A. (1989) *Proc. Natl. Acad. Sci. USA* **86,** 8964–8967.
53. Overton, H. A., Fuji, Y., Price, I. R. & Jones, I. M. (1989) *Virology* **170,** 107–116.
54. Hu, S. L., Travis, B. M., Garrigues, J., Zarling, J. M., Sridhar, P., Dykes, T., Eichberg, J. W. & Alpers, C. (1990) *Virology* **179,** 321–329.
55. Shioda, T. & Shibuta, H. (1990) *Virology* **175,** 139–148.
56. Mergener, K., Fäcke, M., Welker, R., Brinkmann, V., Gelderblom, H. R. & Kräusslich, H. G. (1992) *Virology* **186,** 25–39.
57. Haffar, O., Garrigues, J., Travis, B., Moran, P., Zarling, J. & Hu, S. L. (1990) *J. Virol.* **64,** 2653–2659.
58. Smith, A. J., Cho, M.-I., Hammarskjöld, M.-L. & Rekosh, D. (1990) *J. Virol.* **64,** 2743–2750.
59. Gheysen, D., Jacobs, E., De Foresta, F., Thiriart, C., Francotte, M., Thines, D. & De Wilde, M. (1989) *Cell* **59,** 103–112.
60. Vernon, S. K., Murthy, S., Wilhelm, J., Chanda, P. K., Kalyan, N., Lee, S. G. & Hung, P. P. (1991) *J. Gen. Virol.* **72,** 1243–1251.
61. Royer, M., Cerutti, M., Gay, B., Hong, S.-S., Devauchelle, G. & Boulanger, P. (1991) *Virology* **184,** 487–422.
62. Freed, E. O., Orenstein, J. M., Buckler-White, A. J. & Martin, M. A. (1994) *J. Virol.* **68,** 5311–5320.
63. Chazal, N., Gay, B., Carriére, C., Tournier, J. & Boulanger, P. (1995) *J. Virol.* **69,** 365–375.
64. González, S. A., Affranchino, J. L., Gelderblom, H. R. & Burny, A. (1993) *Virology* **194,** 548–556.
65. Grief, C., Hockley, D. J., Fromholc, C. E. & Kitchin, P. A. (1989) *J. Gen. Virol.* **70,** 2215.
66. Gelderblom, H. R., Özel, M., Hausmann, E. H. S., Winkel, T., Pauli, G. & Koch, M. A. (1988) *Micron. Microsc. Acta* **19,** 41–60.
67. Weiss, C. D., Levy, J. A. & White, J. M. (1990) *J. Virol.* **64,** 5674–5677.
68. Blacklow, S. C., Lu, M. & Kim, P. S. (1995) *Biochemistry* **34,** 14954–14962.
69. Earl, P. L., Doms, R. W. & Moss, B. (1990) *Proc. Natl. Acad. Sci. USA* **87,** 648–652.
70. Pinter, A., Honnen, W. J., Tilley, S. A., Bona, C., Zaghouani, H., Gorny, M. K. & Zolla-Pazner, S. (1989) *J. Virol.* **63,** 2674–2679.
71. Thomas, D. J., Wall, J. S., Hainfeld, J. F., Kaczorek, M., Booy, F. P., Trus, B. L., Eiserling, F. A. & Steven, A. C. (1991) *J. Virol.* **65,** 3797–3803.
72. Schawaller, M., Smith, G. E., Skehel, J. J. & Wiley, D. C. (1989) *Virology* **172,** 367–369.
73. Rao, Z., Belyaev, A. S., Fry, E., Roy, P., Jones, I. M. & Stuart, D. I. (1995) *Nature (London)* **378,** 743–747.
74. Belyaev, A. S., Stuart, D., Sutton, G. & Roy, P. (1994) *J. Mol. Biol.* **241,** 744–746.
75. Matthews, S., Barlow, P., Clark, N., Kingsman, S., Kingsman, A. & Campbell, I. (1995) *Biochem. Soc. Trans.* **23,** 725–728.